**Annales
Geophysicae**

Particle precipitation during NEIAL events: simultaneous ground based nighttime observations at Svalbard

J. Lunde, U. P. Løvhaug, and B. Gustavsson

Department of Physics and Technology, University of Tromsø, Tromsø, Norway

Abstract. In this paper we present Naturally Enhanced Ion Acoustic Lines (NEIALs) observed with the EISCAT Svalbard Radar (ESR) together with auroral emissions observed with the Meridian Scanning Photometer (MSP). This is the first report of NEIALs observed during nighttime at Svalbard. Previously, NEIALs have been associated with a strong red line intensity (>10 kR), which exceeds the green line intensities. The high intensity in the red line emission is a sign of abundant low energy electron precipitation. In our observations, one of the NEIAL events was accompanied by the red line emissions far below the previously reported intensities. This happened when the green line intensity exceeds the red line intensity. In this work we discuss the behaviour of electron precipitation characteristics and optical emissions during NEIAL events on the nightside, and we suggest that intensity enhancements in the 844.6 nm emission line could be a better candidate than the 630.0 nm emission as an optical signature for NEIALs.

Keywords. Ionosphere (Particle precipitation; Plasma waves and instabilities; Polar ionosphere)

1 Introduction

Naturally Enhanced Ion Acoustic Lines are easily distinguishable from the standard thermal incoherent scatter (IS) spectrum due to the very strong enhancement, up to 4–5 orders of magnitude above the thermal level (Grydeland et al., 2004), of one or both ion acoustic shoulders in the power spectrum of the returned signal, see Fig. 1. Such strong enhancements of the ion acoustic frequencies were predicted by Rosenbluth and Rostoker (1962), where they demonstrated theoretically that increased backscatter could be caused by

the growth of ion acoustic waves excited by field-aligned currents (FAC). The normal double-peaked shape of the IS spectra for the F-region backscatter is related to the ratio of electron and ion temperatures being larger than one, while the spectral width reflects the Doppler broadening due to the ion thermal speed. The up-shifted Doppler frequency (right peak/shoulder) and the down-shifted Doppler frequency (left peak/shoulder) correspond to ion-acoustic waves (IAW) propagating towards and away from the receiving radar antenna, respectively. Rietveld et al. (1996) show, by using data from the mainland EISCAT UHF radar, that the left peak is more commonly enhanced at higher altitudes (>450 km) than the right peak and vice versa. Grydeland et al. (2004) show the same by providing a histogram of the occurrence of these echoes at the ESR versus range. Therefore, the enhancement in the down-shifted peak is believed to be associated with soft electron particle precipitation, ion-outflow and upward streaming ionospheric electrons which carry an earthward directed FAC, while the up-shifted peak is interpreted as being associated with downward streaming thermal and supra-thermal electrons as well as ions (Rietveld et al., 1996). For more than a decennium, NEIALs have been interpreted as being caused by i) plasma turbulence driven by short bursts of intense field-aligned currents, the current driven instability (e.g. Foster et al., 1988; Collis et al., 1991; Rietveld et al., 1991), ii) large relative drifts between two or more ion species, the ion-ion two stream instability (e.g. Wahlund et al., 1992b) and iii) nonlinear wave-wave interaction, the parametric decay of Langmuir waves (e.g. Forme, 1993, 1999).

The first observation of NEIALs in the dayside cusp/cleft region using the EISCAT Svalbard Radar (ESR) was reported by Buchert et al. (1999). Later on, more observations have been reported using the ESR (e.g. Sedgemore-Schulthess et al., 1999; Grydeland et al., 2003, 2004; Blixt et al., 2005; Strømme et al., 2005; Ogawa et al., 2006; Lunde et al., 2007). A common feature for all these observations is that they have
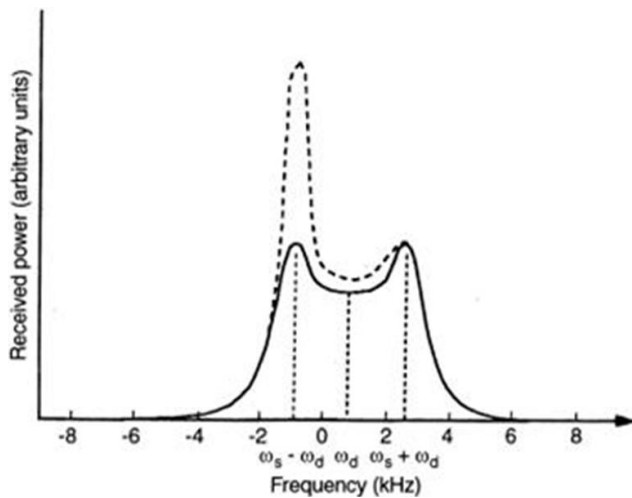
Fig. 1. Theoretical incoherent scatter spectra: classical double-humped shape (solid line) and distorted shape due to ion acoustic fluctuations (dashed line), ω_d is the Doppler shift and ω_s the ion acoustic frequency (Forme and Fontaine, 1999).

been carried out during daytime, and most of them in the vicinity of the dayside cusp/cleft. In contrast, NEIALs reported from the mainland (e.g. Rietveld et al., 1991) have been observed mainly during nighttime in association with the nightside auroral oval. This may not be surprising, since it is well known that the auroral oval is located at higher latitudes for daytime aurora than nighttime aurora. However, during geomagnetic disturbances, the auroral oval can expand both southward and poleward (e.g. Feldstein and Starkov, 1967). In addition, the enhanced radar spectra are generally seen inside or adjacent to regions of strong 630-nm auroral emission, with intensity levels exceeding 10 kR (e.g. Collis et al., 1991), independently of local time. These strong intensities in the red line, occurring simultaneously with NEIALs, have typically been interpreted as a signature of soft particle precipitation. However, the separation between the optical and radar observations has often been significantly larger than the scale size of NEIALs measured by Grydeland et al. (2003, 2004). Also, Collis et al. (1991) point out that it is rare to observe red line auroral emissions which exceed 10 kR, and the occurrence of both NEIALs and bright red emissions appears to be equally rare.

The NEIALs are, in addition to soft particle precipitation (e.g. Collis et al., 1991; Forme et al., 1995) and ion-outflow (e.g. Wahlund et al., 1992a; Forme and Fontaine, 1999), also found to be accompanied with high electron temperatures (e.g. Foster et al., 1988; Wahlund et al., 1993), severe geomagnetic disturbance (e.g. Rietveld et al., 1991), active auroral forms (e.g. Sedgemore-Schulthess et al., 1999; Blixt et al., 2005) and enhanced plasma lines (Strømme et al., 2005). In all these studies, the observations of NEIALs were interpreted as being associated with particle precipitation, directly

or indirectly. Collis et al. (1991) concluded that large fluxes of low energy electrons must be the major cause of NEIALs since they were accompanied by active and intense red auroral forms in the F-region. Forme et al. (1995) found that strong NEIALs were often associated with precipitating particles of energies between 100 eV and 10 keV. Wahlund et al. (1992a) observed NEIALs during short intervals of auroral precipitation and ion outflow (Type II). Forme and Fontaine (1999) found that NEIAL events together with large ion outflows exist inside local turbulent regions characterized by strong electron heating. Foster et al. (1988) showed that large electron to ion temperature ratios, implicit influenced by precipitating particles, could lead to ion acoustic instabilities. Wahlund et al. (1993) observed NEIAL events together with topside ionospheric electron temperature enhancements, and found a good correlation between enhancements in both the electron temperature and the electron density, where the latter enhancement correspond to ionization by electron precipitation in the energy range 100–500 eV. Rietveld et al. (1991) observed NEIALs during severe geomagnetic disturbances with auroral particle precipitation, indicated by electron density enhancement in the E-region. Enhanced IS spectra were also associated with electron heating in the F-region, often large upward plasma flows, auroral arcs and red aurora. Sedgemore-Schulthess et al. (1999) found that NEIAL spectra occur during observations of poleward moving auroral transients and auroral coronal forms, and Blixt et al. (2005) found a strong correlation between NEIALs and dynamic rayed aurora as well as red background emissions, which showed that there is a significant part of low energy electrons among the precipitating electrons. Strømme et al. (2005) found that simultaneous enhancements in the ion- and plasma lines were due to a low energy electron beam (8–80 eV). Furthermore, Robinson et al. (1985) point out a relation between the electron temperature and auroral emissions, as they reported high electron temperatures of 6000 K in association with red aurora. More recently, Lunde et al. (2007) suggested that the electron precipitation energy flux, the characteristic energy and harder precipitation could be of importance in the process of generating NEIALs. Frederick-Frost et al. (2007) suggest that NEIALs and Broad Band Extremely Low Frequency (BBELF, <5 kHz) waves are indicative of the same phenomenon, in which case the parametric decay of Langmuir waves is not a likely explanation.

Based on the literature cited above, there are reasons to believe that NEIALs are associated with particle precipitation (see also Sedgemore-Schulthess and St. Maurice, 2001, and references therein). However, the specific role of for example the energy and/or flux of the precipitation in the process of generating NEIALs is not clear. In this paper, we use optical observations to estimate the electron precipitation characteristics of NEIAL events observed with the ESR during nighttime from Svalbard, with particular emphasis on the 844.6 nm emission line.

27 November 2000   ESR Raw Data
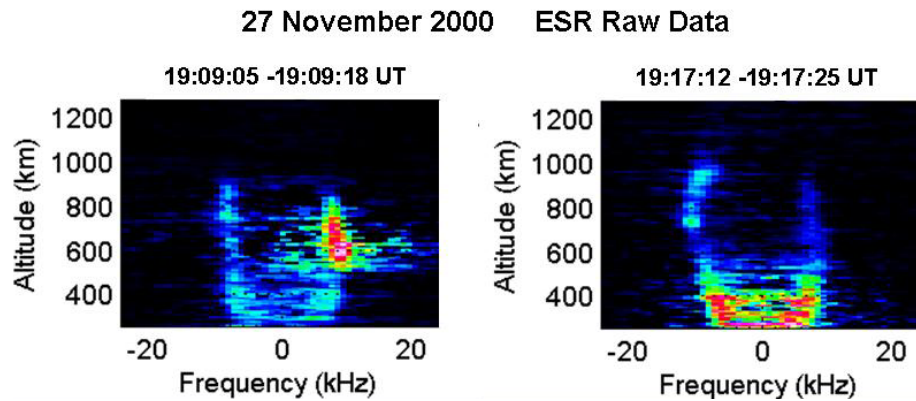
Fig. 2. Examples of NEIALs observed in the raw data. The enhancement in the right shoulder (left panel) corresponds to the time when the green emission line exceeds the red line.

2 Observations

On 27 November 2000, the geophysical conditions indicate an active day with a local K-index for Longyearbyen of about 6 and a westward electrojet just prior to the observed NEIAL events. The Interplanetary Magnetic Field (IMF) was obtained from the ACE satellite (not shown) at the Lagrange point (L1). It was stable for a long time (>8 h) with a strong negative B_Y component (~5 nT), a positive B_X component (~2 nT) and a negative B_Z component (~2 nT) during our time of interest. It should also be mentioned that a Solar Proton Event (SPE) started 24 November (~15:20 UT) with a maximum at 26 November (~20:30 UT) with several associated halo Coronal Mass Ejections (CME) between the morning of the 23rd and afternoon of the 26th.

The ESR (500 MHz) field-aligned 42 m antenna detected 5 periods of enhanced spectra between 18:00–20:00 UT. The radar was operated in a 16 bit alternating code experiment Tau0, version 2.10, with an integration time of 12.8 s. The transmission was switched between the 42 m and 32 m antennas every second integration period. The 32 m antenna was not in a field-aligned position, and no NEIALs were found in that data set. At the same time, auroral emissions were observed with a 5 channel Meridian Scanning Photometer (MSP) every 16 s with an angular resolution of 1°. Since each MSP scan is 16 s, every integrated data dump from the 42 m antenna will be within the time span of the MSP data. Activity was recorded in the following wavelengths: 630.0 nm, red line emission from neutral atomic oxygen, O (^{1}D); 557.7 nm, green line emission from neutral atomic oxygen, O (^{1}S); 427.8 nm, blue line emission from ionized diatomic nitrogen, N_2^+(1NG); 844.6 nm, near infrared line emission from neutral atomic oxygen, O ($3p^3$P); and 486.1 nm, Balmer line emission from neutral hydrogen, H_β. However, the Balmer line emission was very weak and noisy; hence emissions caused by proton precipitation will not contribute significantly to the observed auroral emissions. The photometer was located at the Auroral Station in

Adventdalen, Longyearbyen, Svalbard, close to the ESR site (~7 km). The geographic coordinates for the radar facility is 78.15° N and 16.03° E, while the corrected geomagnetic coordinates from the IGRF-2000 is 75.17° N and 112.28° E, which gives a magnetic midnight at ~20:48 UT. The field-of-view of the radar and the MSP overlap at E- and F-region heights.

In the raw data we observe NEIALs in 4 individual data dumps (19:02:16–19:02:29 UT; 19:09:05–19:09:18 UT; 19:19:20–19:19:33 UT; 19:23:36–19:23:49 UT) and in 5 consecutive data dumps (19:15:55–19:17:50 UT). Because of the integration time we are not able to measure NEIAL events on shorter time scales, but it is known that they can appear on time scales of less than 1 s (Grydeland et al., 2004). Figure 2 shows two examples of NEIALs in the raw-data spectra. The left panel shows a very distinct enhancement in the right shoulder, which will be further discussed. We observe enhancements in the left, right and both shoulders during the time of interest. An example of the latter is shown in the right panel of Fig. 2.

Figure 3 shows the analysed data from the 42 m antenna. The standard analysis estimates electron density, electron- and ion temperatures and ion drift, provided the backscattered signal is from a thermal plasma. During NEIALs events, this is not a valid assumption and the electron density and temperature estimates are therefore not representative for the ionosphere. Instead, the analyzed data indicates that we are dealing with highly non-thermal spectra. It can clearly be seen in Fig. 3 between ~19:00–19:25 UT (encapsulated by 5 black ovals, which show the time of NEIAL events), that the electron temperature is high (>6000 K) while the ion temperature is not particularly enhanced. In addition, ion outflow is seen at high altitudes as well as increased electron density ($>10^{12}$ m^{-3}) for some of the events. The ratio T_e/T_i is increased from about 1.3 outside the NEIAL events to more than 2 within them. All these factors at the same time have previously been taken as signatures of NEIALs.
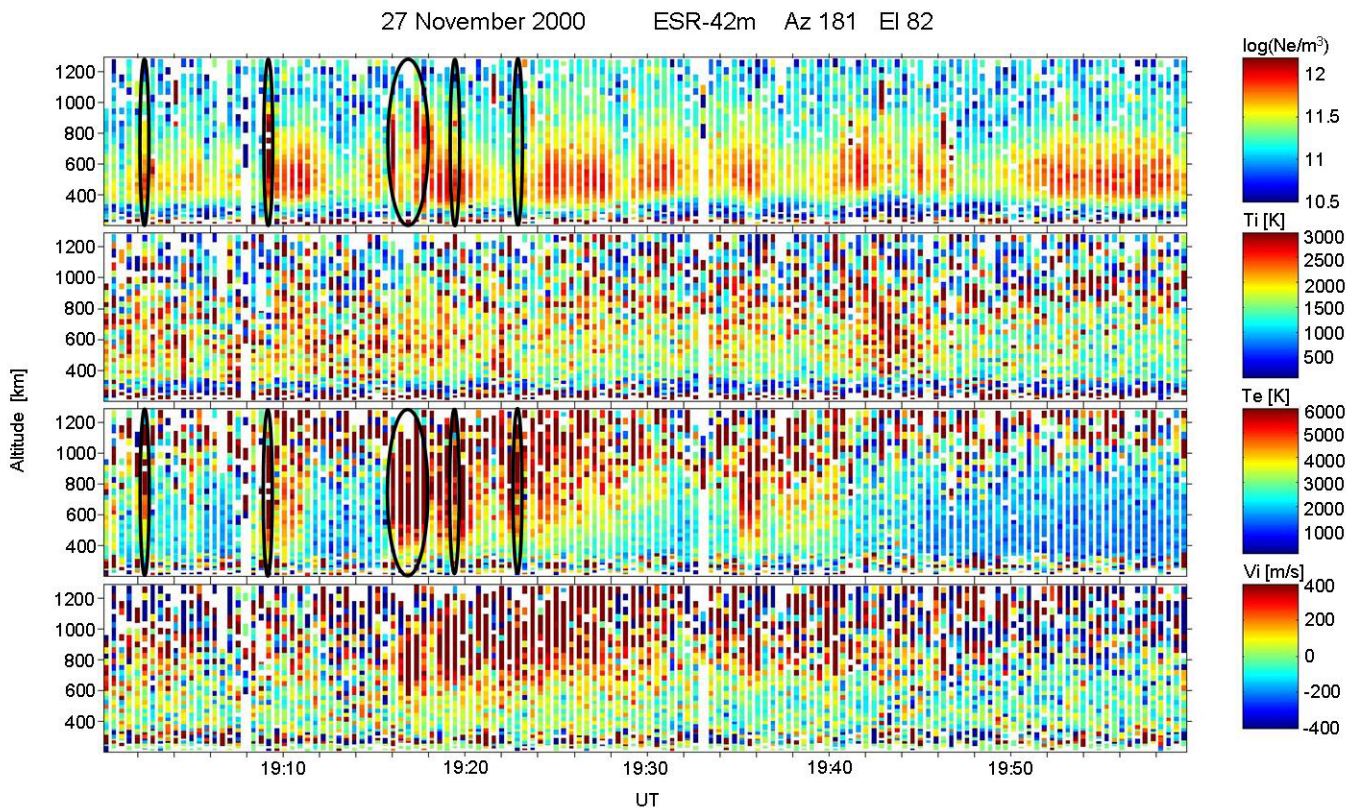
Fig. 3. A standard analysis of the ESR data where the panels show from the top to the bottom: the electron density, the ion temperature, the electron temperature and the ion drift velocity, respectively. The time of the NEIAL events is encapsulated by black ovals.

Figure 4 shows the column emission rates of 630.0 nm, 427.8 nm, 557.7 nm and 844.6 nm versus time and scan angle, where ~98° corresponds to the intersection with the 42 m beam (dashed white line). The MSP shows a typical substorm signature, seen as a rapid poleward expansion starting at ~18:53 UT which reaches the northernmost latitude at ~18:57 UT. This gives a rapid poleward expansion velocity which increase from about 1 to 2 km/s. Furthermore, during the recovery phase, seen as the equatorward motion, another onset happens at ~19:15 UT. From ~19:16 UT to ~19:18 UT, five consecutive data dumps with NEIALs are observed, and afterwards two more NEIAL events happen at ~19:19 UT and ~19:24 UT. In Fig. 4, between 19:00–19:40 UT (encapsulated with black ellipse), 3 small and distinct intensifications are seen above Longyearbyen for all wavelengths; ~19:02 UT, ~19:09 UT and ~19:34 UT.

In addition, we also looked at data from the magnetometer network IMAGE (International Monitor for Auroral Geomagnetic Effects) and the Cutlass radars (8–20 MHz), a part of the Super Dual Auroral Radar Network (SuperDARN). The latter show the characteristic two-cell patterns of ionospheric convection (Fig. 5), due to a southward IMF ($B_z < 0$). The plasma convection speed in the ionosphere observed by the SuperDARN radar was about 1 km/s in the eastward di-

rection (dawn-dusk) and the convection flow was equatorward (moving towards the Sun). The magnetograms from the IMAGE network, with 20 s resolution data, show a clear negative deflection at Longyearbyen of ~425 nT in the horizontal component at ~18:53 UT (Fig. 6), which is about 10 min before the first NEIAL observation. Also, poleward propagation is clearly seen in Fig. 6 (illustrated with green and blue triangles), which gives a poleward expansion velocity similar to that obtained from the MSP data, and which is of the order of typical plasma convection speed in the ionosphere. Additionally, the ionospheric equivalent current estimated from MIRACLE, a two-dimensional instrument network for mesoscale studies of auroral electrodynamics (www.space.fmi.fi/MIRACLE/index.html), shows periods of eastward and westward current enhancement between 18:15–18:45 UT and 18:25–19:00 UT, respectively. The region of eastward current enhancement occurs between 64.5°–69.5° N geographic latitude, and is strongest between 67°–69.5° N, while the westward current enhancement occurs between 72°–79° N geographic latitude, strongest between 73°–78° N.
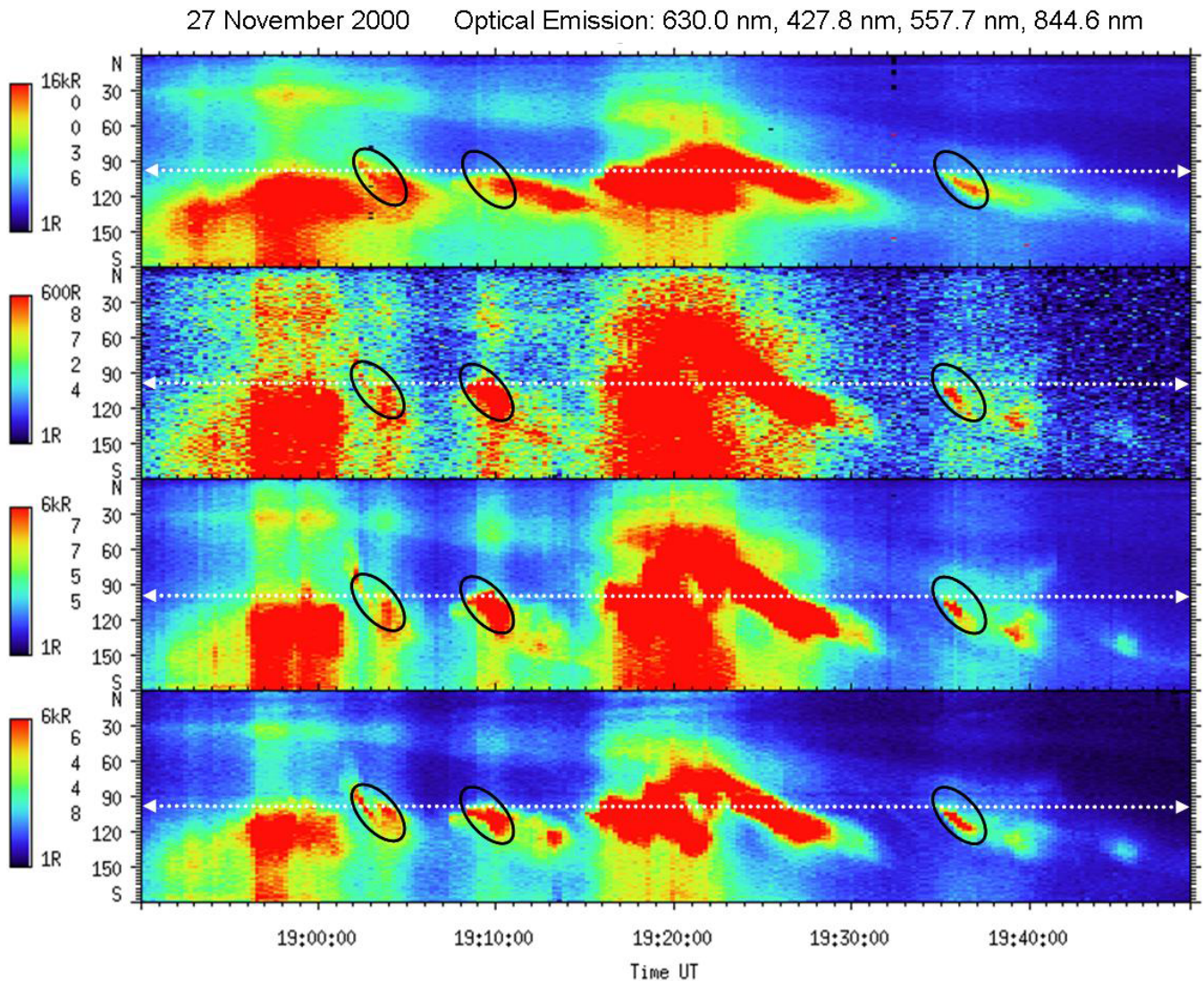
Fig. 4. An overview of the recorded emission intensity by the MSP in Rayleigh versus time and scan angle for the 630.0 nm, 427.8 nm, 557.7 nm and 844.6 nm lines. The white dashed line represents the intersection with the radar field of view. The black ovals encapsulate 3 small and distinct separated formations.

3 Discussion

In Fig. 4, the 2 small intensifications at ∼19:02 UT and ∼19:09 UT match the times of the NEIAL events; in particular, the first intensification matches the first observed NEIAL event, while the second intensification matches the event where the green line intensity exceeds the red line intensity. Figure 7 shows how the optical intensities vary inside the radar field of view. The black arrows indicate the times we observe NEIALs in the radar data (∼19:02 UT, ∼19:09 UT, ∼19:19 UT, ∼19:24 UT), and the black diamond (at the top and in the middle of the figure) represents the five consecutive NEIAL events (∼19:16–19:18 UT), while the notation (a, b, c, d) illustrate some cases where the red line emission intensification peak does not correspond to any

NEIAL observations (∼18:57 UT, ∼19:21 UT, ∼19:23 UT, ∼19:34 UT). The events chosen for comparison (a–d) represent large rapid intensity increases in the red line. In all NEIAL events, except for the one at ∼19:09 UT, the red line intensity (>10 kR) is greater than the green line intensity. The exception is enclosed in a frame (Fig. 7). This event corresponds to strong backscatter in the right shoulder of the incoherent scatter spectrum. The dynamic range of the optical intensities during periods of NEIAL events is found to be: 6.6–36.3 kR for 630.0 nm, 4.5–14.9 kR for 557.7 nm, 0.56–1.67 kR for 427.8 nm and 4.5–18.7 kR for 844.6 nm. We see that the 844.6 nm emission line intensity is below the dynamic range at ∼18:57 UT (a), ∼19:21 UT (b), ∼19:23 UT (c) and ∼19:34 UT (d). The line intensities of 630.0 nm,
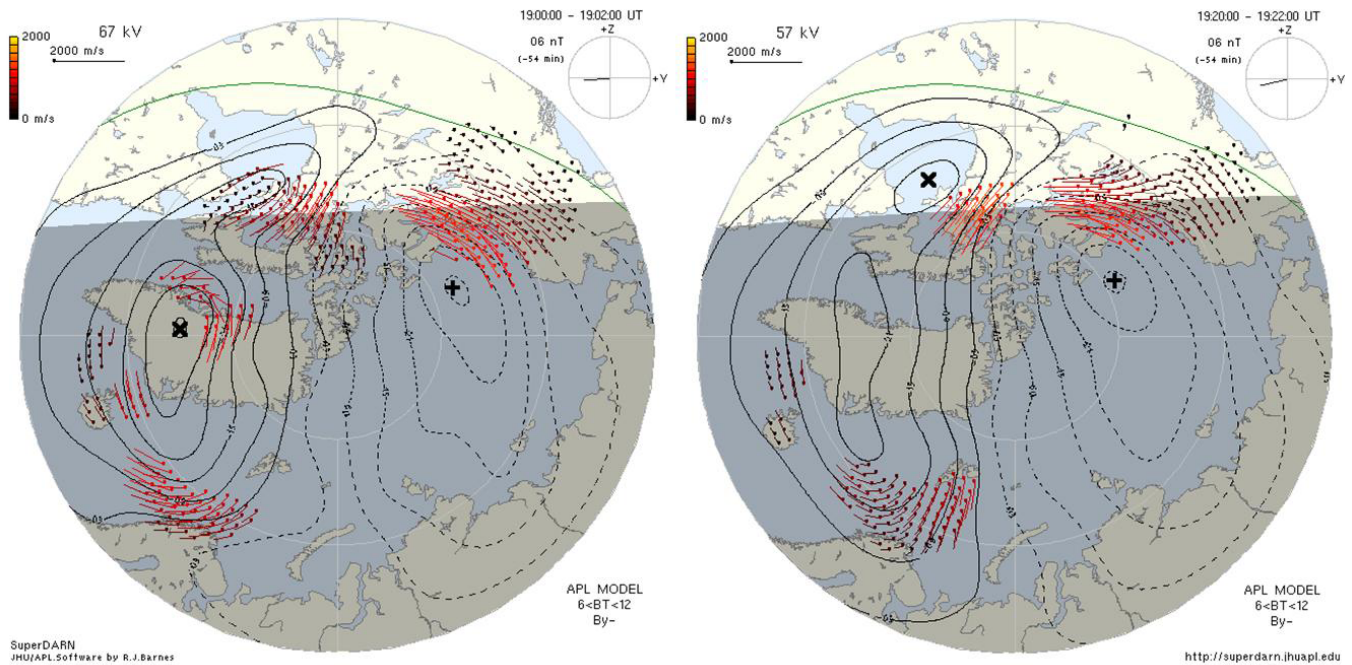
Fig. 5. SuperDARN plasma convection data are shown for 19:00:00–19:02:00 UT (left) and 19:20:00–19-22:00 UT (right).

557.7 nm and 427.8 nm emissions are below the dynamic range only at ∼19:34 UT (d). The previously assumed requirement that the intensity of the 630.0 nm line should be above about 10 kR (Collis et al., 1991) is an insufficient criterion for NEIALs to be detected by the ESR. The peaks a), b) and c) in Fig. 7 are all above 10 kR, but no NEIALs were detected. On the other hand, we note that the 844.6 nm intensities are very low during these events. In addition, the electron energy flux is found to be insufficient (less than 2.4 mW/m^2, see discussion below) at ∼18:57 UT (a), ∼19:23 UT (c) and ∼19:34 UT (d). In Fig. 7, the example (d) is close to the small equatorward intensification, seen around ∼19:34 UT in Fig. 4. This feature at first sight implies a possible NEIAL event due to the apparent intensifications similar to the occurrences at ∼19:02 UT and ∼19:09 UT. Unfortunately, this enhancement appears adjacent to the local magnetic zenith and just on the edge of the radar field of view and the ESR does not record a NEIAL event around that time. The fact that Fig. 4 shows clear intensifications in event d) and that we do not see NEIALs in the radar beam suggests that NEIALs are small-scale structures directly tied to the spatial extent of the auroral precipitation.

In general, the intensity of the 427.8 nm emissions allows us to deduce the total energy flux of the precipitating electrons, while intensity ratios (e.g. 630.0/427.8, 844.4/427.8 and 557.7/427.8) are related to the characteristic or mean energy of the primary precipitating electrons. To estimate the energy flux and characteristic energy we use the method

described by Lunde et al. (2007) and references therein. By using ground based optical data, we find that the minimum electron energy flux during NEIAL events for this case study is ∼2.4 mW m^{-2}, while the average flux between 18:00–20:00 UT is about 1 mW m^{-2}. The minimum energy flux is somewhat lower compared to earlier observations (∼3.4 mW m^{-2}) in the cusp study (Lunde et al., 2007), but still, within this case study the values are clearly different when NEIALs are present compared to when they are or not. This implies that it is important to use the values of the energy flux as a reference from case to case rather than an absolute reference. At least, the electron energy flux of soft particles is expected to be larger for daytime than nighttime observations. The characteristic energy ∼60–300 (∼158 eV in average) is approximately in the same range as found in the cusp study ∼50–220 eV (∼115 eV in average) (Lunde et al., 2007). Regarding the emission line intensities, compared to the cusp result, the red and blue line intensities are lower, while the green and infrared intensities are greater. It should be noted that the intensity ratio between 557.7 nm and 844.6 nm shows a high similarity to the ratio during the cusp event, both with respect to the maximum (∼5) and minimum (∼0.6) values as well as the values during NEIAL events (∼0.6–1.8). The other intensity ratios were not to any great extent comparable, but still, the NEIALs occur within the dynamic range representative for each of the cases.

Figure 8 is a MSP plot showing the intensity of the 844.6 nm emission line versus time and scan angle, where the

black arrows correspond to the NEIAL events and the white arrows with notations (a-c, which correspond to Fig. 7) represent absence of NEIALs. The figure shows that the 844.6 nm line may be a more suitable candidate than the 630.0 nm for discriminating when NEIALs are observed or not. Both lines are emitted by atomic oxygen (OI). Since the transition emitting at 630.0 nm is forbidden (with a radiative lifetime of 107 s) it is strongly influenced by quenching, leading to an effective lifetime varying with altitude, typically 25–40 s at 200–300 km altitude. The 844.6 nm is a prompt emission (20 ns). Thus, the 844.6 nm line responds instantaneously to temporal changes in the auroral precipitation (Vallance Jones et al., 1987). The 844.6 nm emissions are produced by two processes; where the direct impact of electron on O atoms is dominant, while dissociative excitation of O_2 molecules occurs during large storms (Strickland et al., 1989). The dissociative recombination is expected to contribute with 27% during nighttime conditions (Christensen et al., 1983). The optical observations strongly indicate that the red line intensity alone is not a sufficient criterion for NEIALs to occur. If that was the case, more observed NEIAL events should be expected, as for example in the whole period from 19:16–19:26 UT, where the red line emissions are well above 10 kR (see Figs. 4 and 7). By looking closer at the other emission lines than 630.0 nm, especially the 844.6 nm line, the lack of NEIALs in the radar data corresponds to the rapid decay from a high intensity to a lower intensity, seen as "gaps" in Fig. 8 and valleys in Fig. 7. Rapid intensifications in the 844.6 nm emission seem to be a good indicator of NEIAL activity. Both 844.6 nm and 630.0 nm are efficiently excited by low energy precipitation.

The increased auroral activity follows a poleward propagation of the magnetic deflection (electrojet) seen as a clear negative bay of ~425 nT in the horizontal component in the IMAGE magnetometer at Longyearbyen at ~18:53 UT (Fig. 6), about 10 min before the first NEIAL observation. It is worth noting that this is consistent with previous reported results from the cusp region (Lunde et al., 2007). In addition, the westward electrojet is related to the negative B_Y, and this situation together with poleward expansion events, which are seen in both the IMAGE and photometer data, are typical signatures of a substorm expansion phase (e.g. Rostoker, 1996). The local K-index of 6 matches very well with previously reported events (Rietveld et al., 1996; Ogawa et al., 2006; Lunde et al., 2007), which showed NEIAL events during periods with the K-index larger than 4.

From the data discussed above, it is difficult to clearly distinguish between the Langmuir decay – and the current driven instability theory. We observe that all NEIALs in this experiment are associated with enhancements in 844.6 nm emission line, which is related to soft particle precipitation. On the other hand, we have an event where the green line exceeds the red line intensity, and this causes an enhancement in the up-shifted shoulder. This is in accordance with the explanation put forward by Rietveld et al. (1991), who
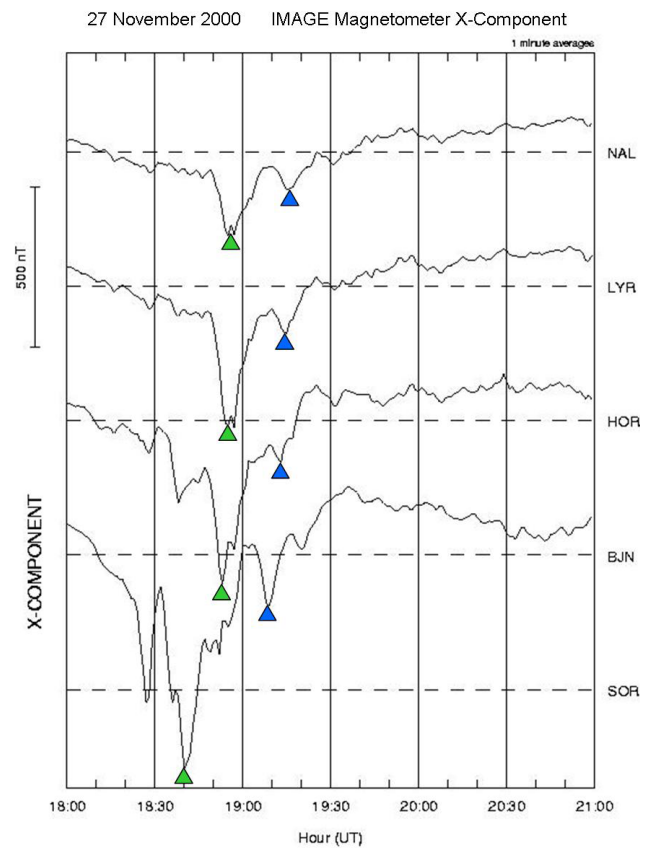

Fig. 6. Magnetogram for the X-component at 5 different stations from 18:00–21:00 UT: Sørøya (SOR, 67.34° N), Bjørnøya (BJN, 71.43° N), Hornsund (HOR, 74.12° N), Longyearbyen (LYR, 75.23° N) and Ny Ålesund (NAL, 76.17° N). All latitudes are given in Corrected GeoMagnetic (CGM) coordinates from the year 2000. The green and blue triangles correspond to a substorm onset and the apparent subsequent poleward expansion, respectively.

state that the enhancement in the right shoulder is due to the precipitation of thermal and suprathermal electrons. Our NEIAL events are observed during periods with the K-index larger than 4, and enhanced electrojets are detected by MIRACLE. Rino, already in 1972 reported observations of spectral asymmetries in association with electrojet currents. This, together with the substorm expansion phase discussed above, indicates that a large current system is present. Within such large scale currents, together with sharp gradients in conductivities such as auroral arcs, small intense FAC's are expected (Nöel et al., 2000) and observed (Neubert et al., 2003). During particle precipitation, a parallel electric field is set up, and Gudkova et al. (1973) predict a rapid increase in the electron temperature due to the onset of the Buneman instability when a parallel electric field is associated with the FAC region. The resulting turbulence acts to inhibit the free acceleration of electrons relative to the ions and the plasma rapidly becomes strongly non-isothermal ($T_e/T_i \gg 1$), which leads to an ion acoustic instability (Foster et al., 1988).
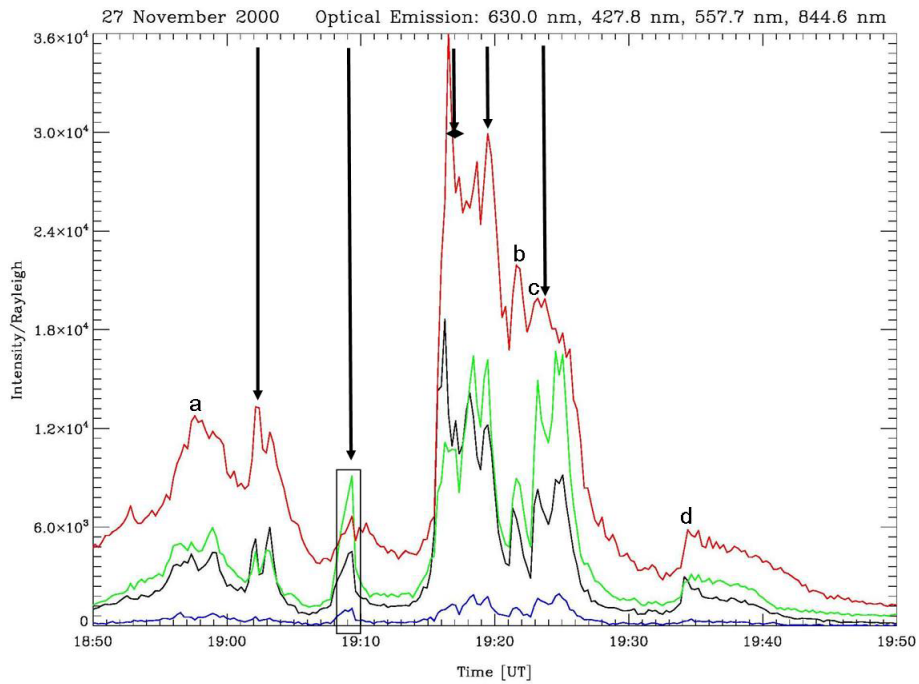
Fig. 7. Optical emissions corresponding to the field-aligned radar beam direction between 18:00–20:00 UT and the MSP meridian scans have been smoothed by using a weighted triangular filtering of ±1°. NEIAL events are marked with black arrows (and a black diamond), while the notation a, b, c and d shows emission peaks which do not correspond to such events. The enclosed frame is the event where the green line intensity exceeds the red line. The colour code is red, green, black and blue for the 630.0 nm, 557.7 nm, 844.6 nm and 427.8 nm lines, respectively.
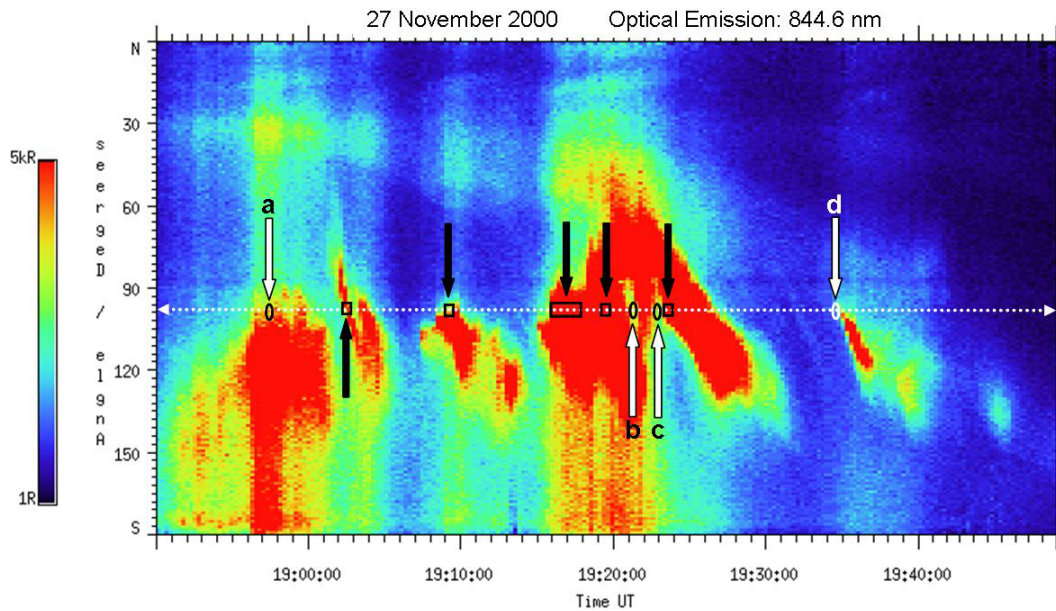
Fig. 8. The MSP plot shows the Rayleigh intensity of the 844.6 nm emission line versus time and scan angle. The white dashed line represents the intersection with the radar field of view. The frames indicate the duration of NEIALs. The black arrows, together with the frames, correspond to NEIAL events, while white arrows together with ellipses indicate the absence of NEIALs. At the 3 first white arrows, the red line emissions are well above 10 kR, while the 844.6 nm emission is below the dynamic range. The notations: a, b, c and d are the same as in Fig. 7.

In our case we observe enhancements in single shoulders as well as in both shoulders in individual data dumps. The NEIAL events are believed to vary on a timescale down to less than a second, according to results by Grydeland et al. (2004), but because of the poor time resolution in our experiment (integration time of 12.8 s), it is impossible to state whether we have enhancements in both shoulders at the very same time or not. The enhancement in both shoulders simultaneously has previously been interpreted as not being due to the current driven instability, since this would require intense, oppositely directed current pairs within the radar beam width (e.g. Rietveld et al., 1991). However, Collis et al. (1991) suggested that enhancements in both shoulders simultaneously are possible during the current driven instability process. Neubert et al. (2003) have demonstrated that intense, small-scale FACs indeed exists. More recently, Daldorff et al. (2007) show by modelling that the oscillating two-stream instability driven by a cold electron beam is a possible theory for the generation of NEIALs.

4   Conclusions

This paper shows that NEIALs are also a phenomenon which may be observed during nighttime hours at high latitudes in Svalbard. The geophysical settings indicate that the NEIAL events in this case study are associated with the substorm expansion phase on the nightside. We have also found that the green line may exceed the red line intensity during NEIAL events, causing enhancement in the up-shifted shoulder in the incoherent scatter spectra. This shows that both soft and hard precipitation is essential for the generation of NEIALs; the harder precipitation being important for the enhancement in the up-shifted ion-acoustic line. We also find that the enhancement of the down-shifted shoulder is not strictly related to the previous threshold of about 10 kR for the 630.0 nm line intensities. There seems to be a possible link between the NEIAL events and the 844.6 nm line emission intensity which probably makes this line a more suitable indicator of NEIAL activity than the 630.0 nm emission line. Both the 630.0 nm and 844.6 nm are emitted by atomic oxygen (OI), excited by low energy precipitation, but the latter results from a prompt emission, and shows a better correlation with NEIALs on the short time scales involved.

References

Blixt, E. M., Grydeland, T., Ivchenko, N., Hagfors, T., La Hoz, C., Lanchester, B. S., Løvhaug, U. P., and Trondsen, T. S.: Dynamic rayed aurora and enhanced ion-acoustic radar echoes, Ann. Geophys., 23, 3–11, 2005, http://www.ann-geophys.net/23/3/2005/.

Buchert, S. C., van Eyken, A. P., Ogawa, T., and Watanabe, S.: Naturally enhanced ion-acoustic lines seen with the EISCAT Svalbard Radar, Adv. Space Res., 23, 1699–1704, 1999.

Chen, F. F.: Introduction to Plasma Physics and Controlled Fusion, vol. 1, 2nd ed., Plenum, New York, 1984.

Christensen, A. B., Sivjee, G. G., and Hecht, J. H.: O I (7990 Å) Emission and Radiative Entrapment of Auroral EUV, J. Geophys. Res., 88, 4911–4917, 1983.

Collis, P. N., Häggström, I., Kaila, K., and Rietveld, M. T.: EISCAT radar observations of enhanced incoherent scatter spectra; their relation to red aurora and field-aligned currents, Geophys. Res. Lett., 18, 1031–1034, 1991.

Daldorff, L. K. S., Pécseli, H. L., and Trulsen, J.: Nonlinearly generated plasma waves as a model for enhanced ion acoustic lines in the ionosphere, Geophys. Res. Lett., 34, L18101, doi:10.1029/2007GL031513, 2007.

Feldstein, Y. I. and Starkov, G. V.: Dynamics of auroral belt and polar geomagnetic disturbances, Planet. Space Sci., 15, 209–229, 1967.

Forme, F. R. E.: A new interpretation on the origin of enhanced ion acoustic fluctuations in the upper ionosphere, Geophys. Res. Lett., 20, 2347–2350, 1993.

Forme, F. R. E.: Parametric decay of beam-driven Langmuir wave and enhanced ion-acoustic fluctuations in the ionosphere: a weak turbulence approach, Ann. Geophys., 17, 1172–1181, 1999, http://www.ann-geophys.net/17/1172/1999/.

Forme, F. R. E., Fontaine, D., and Wahlund, J. E.: Two different types of enhanced ion acoustic fluctuations observed in the upper ionosphere, J. Geophys. Res., 100, 14625–14636, 1995.

Forme, F. R. E. and Fontaine, D.: Enhanced ion acoustic fluctuations and ion outflows, Ann. Geophys., 17, 182–189, 1999, http://www.ann-geophys.net/17/182/1999/.

Foster, J. C., del Pozo, C., Groves, K., and St. Maurice, J.-P.: Radar observations of the onset of current driven instabilities in the topside ionosphere, Geophys. Res. Lett., 15, 160–163, 1988.

Frederick-Frost, K. M., Lynch, K. A., Kintner Jr., P. M., Klatt, E., Lorentzen, D., Moen, J., Ogawa, Y., and Widholm, M.: SERSIO: Svalbard EISCAT Rocket Study of Ion Outflows, J. Geophys. Res., 112, A08307, doi:10.1029/2006JA011942, 2007.

Grydeland, T., La Hoz, C., Hagfors, T., Blixt, E. M., Saito, S., Strømme, A., and Brekke, A.: Interferometric observations of filamentary structures associated with plasma instability in the auroral ionosphere, Geophys. Res. Lett., 30, 1338, doi:10.1029/2002GL016362, 2003.

Grydeland, T., Blixt, E. M., Løvhaug, U. P., Hagfors, T., La Hoz, C., and Trondsen, T. S.: Interferometric radar observations of filamented structures due to plasma instabilities and their relation to dynamic auroral rays, Ann. Geophys., 22, 1115–1132, 2004, http://www.ann-geophys.net/22/1115/2004/.

Gudkova, V. A., Zelenyy, L. M., and Liperovskiy, V. A.: Dynamics of longitudinal currents in the magnetosphere, Geomag. and Aeron., 13, 272–277, 1973.

Lunde, J., Gustavsson, B., Løvhaug, U. P., Lorentzen, D. A., and Ogawa, Y.: Particle precipitations during NEIAL events: simul-

taneous ground based observations at Svalbard, Ann. Geophys., 25, 1323–1336, 2007,
http://www.ann-geophys.net/25/1323/2007/.

Neubert, T. and Christiansen, F.: Small-scale, field-aligned currents at the top-side ionosphere, Geophys. Res. Lett., 30, 2010, doi:10.1029/2003GL017808, 2003.

Noël, J.-M. A., St.-Maurice, J.-P., and Blelly, P.-L.: Nonlinear model of short-scale electrodynamics in the auroral ionosphere, Ann. Geophys., 18, 1128–1144, 2000,
http://www.ann-geophys.net/18/1128/2000/.

Ogawa, Y., Buchert, S. C., Fujii, R., Nozawa, S., and Forme, F.: Naturally enhanced ion-acoustic lines at high altitudes, Ann. Geophys., 24, 3351–3364, 2006,
http://www.ann-geophys.net/24/3351/2006/.

Rietveld, M. T., Collis, P. N., and St.-Maurice, J.-P.: Naturally Enhanced Ion Acoustic Waves in the Auroral Ionosphere Observed With the EISCAT 933-MHz Radar, J. Geophys. Res., 96, 19291–19305, 1991.

Rietveld, M. T., Collis, P. N., van Eyken, A. P., and Løvhaug, U. P.: Coherent echoes during EISCAT UHF Common Programmes, J. Atmos. Terr. Phys., 58, 161–174, 1996.

Rino, C. L.: Radar measurement of ionospheric motion in the presence of current-induced spectral asymmetries, Radio Sci., 7, 1049–1060, 1972.

Rosenbluth, M. N. and Rostoker, N.: Scattering of electro magnetic waves by a nonequilibrium plasma, Phys. Fluids, 5, 776–788, 1962.

Robinson, R. M., Mende, S. B., Vondrak, R. R., Kozyta, J. U., and Nagy, A. F.: Radar and photometric measurements of an intense type A red aurora, J. Geophys. Res., 90, 457–466, 1985.

Rostoker, G.: Phenomenology and physics of magnetospheric substorm, J. Geophys. Res., 101, 12955–12973, 1996.

Sedgemore-Schulthess, K. J. F., Lockwood, M., Trondsen, T. S., Lanchester, B. S., Rees, M. H., Lorentzen, D. A., and Moen, J.: Coherent EISCAT Svalbard Radar spectra from the dayside cusp/cleft and their implication for transient field-aligned currents, J. Geophys. Res., 104, 24613–24624, 1999.

Sedgemore-Schulthess, F. and St.-Maurice, J.-P.: Naturally enhanced ion-acoustic spectra and their interpretation, Surv. Geophys., 22, 55–92, 2001.

Strickland, D. J., Meier, R. R., Hecht, J. H., and Christensen, A. B.: Deducing Composition and Incident Electron Spectra From Ground-Based Auroral Optical Measurements: Theory and Model Results, J. Geophys. Res., 94, 13527–13539, 1989.

Strømme, A., Belyey, V., Grydeland, T., La Hoz, C., Løvhaug, U. P., and Isham, B.: Evidence of naturally occurring wave-wave interactions in the polar ionosphere and its relation to naturally enhanced ion acoustic lines, Geophys. Res. Lett., 32, L05103, doi:10.1029/2004GL020239, 2005.

Vallance Jones, A., Gattinger, R. L., Shih, P., Meriwether, J. W., Wickwar, V. B., and Kelly, J.: Optical and Radar Characterization of a Short-Lived Auroral Event at High Latitude, J. Geophys. Res. 92, 4575–4589, 1987.

Wahlund, J. E., Opgenoorth, H. J., Häggström, I., Winser, K. J., and Jones, G. O. L.: EISCAT Observations of the Topside Ionospheric Ion Outflows During Auroral Activity: Revisited, J. Geophys. Res., 97, 3019–3037, 1992a

Wahlund, J.-E., Forme, F. R. E., Opgenoorth, H. J., Persson, M. A. L., Mishin, E. V., and Volokitin, A. S.: Scattering of electromagnetic waves from a plasma: enhanced ion acoustic fluctuations due to ion-ion two-stream instabilities, Geophys. Res. Lett., 19, 1919–1922, 1992b.

Wahlund, J.-E., Opgenoorth, H. J., Forme, F. R. E., Persson, M. A. L., Häggström, I., and Lilensten, J.: Electron energization in the topside auroral ionosphere: on the importance of ion-acoustic turbulence, J. Atmos. Terr. Phys., 55, 623–645, 1993.